MICROFLUIDIC SENSOR FOR WHITE BLOOD CELL COUNTING AND FLOW METERING

BY

UMER HASSAN

THESIS

Submitted in partial fulfillment of the requirements
for the degree of Master of Science in Electrical and Computer Engineering
in the Graduate College of the
University of Illinois at Urbana-Champaign, 2013

Urbana, Illinois

Adviser:

Professor Rashid Bashir

ABSTRACT

Cell counting finds many applications in diagnostics of many diseases. One of the most common tests recommended by the physicians is Complete Blood Cell Count (CBC). For example, there is a decrease in the platelet count in case of Dengue fever. Red blood cells decrease in the case of anemia. CD4 T cells decrease in the case of HIV/AIDS. Cell counting in general, and ability to count the specific cells, would greatly help in clinical diagnostics. Currently, flow cytometers are used for this purpose, but they have not been able to penetrate in the resource-limited settings around the world because of being expensive and because they require trained technicians to operate. Over many years, people have developed microfluidic devices for cell counting, which could provide a portable and economical solution to the problem of cell counting at point-of-care.

In this report, we present a technique for counting the white blood cells and differentiating some of its sub-types within a microfluidic device. Starting with the whole blood, the red blood cells are lysed by saponin and formic acid. Quenching solution composed of phosphate buffer saline is infused in the device to halt the lysing process and maintain the pH of the solution. The remaining white blood cells are then passed across micro-fabricated electrodes within a microfluidic channel. The impedance is measured at 303 kHz and 1.7 MHz signals. The height of the pulse is proportional to the size of the cell. By selecting the appropriate threshold, the number of the cells can be calculated, and white blood cell sub-types can be differentiated based on their size.

Lysed blood flow metering is also possible using the same setup. The width of the pulse for each passage of the cell through the electrode is proportional to the speed of the

cell. By investigating the pulse width, the flow rate can be monitored. Similarly, with increasing flow rates, the baseline amplitude measured in between the electrodes is also proportional to the flow rate.

This device has the potential for use in counting specific types of white blood cells. In particular, we are currently characterizing the device for counting of CD4+ and CD8+ T lymphocytes, which are the primary diagnostics biomarkers for HIV/AIDS.

ACKNOWLEDGMENTS

I would like to thank my adviser, Prof. Rashid Bashir, for providing me this great opportunity to work in his research group and allowing me to work on this significant project of global health impact. I am thankful to him for his guidance, support, and invaluable discussions on the topic. I highly appreciate the help and guidance of Nicholas N. Watkins, from whom I learned a lot during my early stage of graduate studies. I would also like to thank Gregory Damhorst, HengKan Ni, and Chelsea E. Edwards for their help in the project.

I give my deepest thanks to my parents, Seemi Shahid and Shahid Iqbal Siddiqui, for their prayers, love and guidance at every stage of my life. I would like to thank my fiancé, Saba for being a very important part of my life. Finally, I would like to thank my Creator for giving me the knowledge, wisdom and His blessings throughout my life.

TABLE OF CONTENTS

CHAPTER 1 INTRODUCTION……..1

1.1. Introduction to Cell Counting……...1
1.2. Flow Cytometry……2
1.2.1. Drawbacks……....3
1.3. Coulter Counting Principle……4
1.3.1. Effect of the coincident particles……5
1.4. Electrical Counting of Cells...……6
1.4.1. Transmembrane voltage of a cell……6
1.4.2. Electrical model of a cell……..……8
1.4.3. Electrical double layer capacitance……11
1.5. Forces on a Particle in a Microfluidic Flow……12

CHAPTER 2 ELECTRICAL COUNTING OF SPECIFIC WHITE BLOOD CELLS..16

2.1. Microfluidics and Lab-on-a-Chip……16
2.1.1. Key criteria……....16
2.2. Composition of Human Blood……..17
2.3. Experimental Approach……...17
2.3.1. Cell counting approach……..……17
2.4. Electrical Counting of Cells……19
2.4.1. Analysis of counts……..21
2.5. Validation of Electrical Counts (Comparison with Optical Counts)……22
2.6. Cell Viability Analysis……23
2.6.1. Single counter approach……...……..24
2.6.2. Dual counter approach……26
2.7. Experimental Setup……...28
2.8. Fabrication……29
2.8.1. Electrodes fabrication protocol……...29
2.8.2. Fluidics mask fabrication……30

CHAPTER 3 FLOW METERING OF BLOOD IN A MICROFLUIDIC DEVICE…...32

3.1. Introduction ……..32
3.2. Electrical Flow Metering……...33
3.3. Flow Metering of Lysed Blood..……...34
3.3.1. Experimental method……..34
3.4. Results……...36
3.4.1. Flow rate vs. cell counting……..……...36
3.4.2. Flow rate measurement using pulse width……37
3.5. Conclusion……40

CHAPTER 4 FUTURE WORK……41

4.1. CD4 and CD8 T Cell Counter with Flow Metering..……..41
4.2. Complete Blood Cell Count……43

REFERENCES……45

APPENDIX DATA ANALYSIS ……..…….50

A.1 Pulse Counting Based on Threshold….....50
A.2 Dual Frequency Measurement...……...53
A.3 Main Project File…...……...53

CHAPTER 1
INTRODUCTION

1.1. Introduction to Cell Counting

Cell counting finds many applications in diagnostics of many diseases. One of the most common tests recommended by the physicians is Complete Blood Cell Count (CBC). Cell counting would be highly useful in Acute Radiation Syndrome (ARS) where White Blood Cell (WBC) differential is required for its rapid management of the disease. In chemotherapy and radiation therapy, the blood cell production needs to be monitored. Inflammation, leukemia, tissue injury, bone marrow failure, and immunodeficiency can be identified by the irregular total WBC and its differential count. Similarly, bone marrow fibrosis, lymphoma, aplastic anemia, and lupus erythematous are associated with abnormal platelet counts. Excessive bleeding, kidney bleeding, cancer, and mechanical trauma can be identified by the Red Blood Cell (RBC) count [1].

The cell counting in general and ability to count the specific cells would greatly help in diagnostics. Currently, flow cytometers are used for this purpose, but they have not been able to penetrate in the resource limited settings around the world because of being expensive and requiring trained technicians to operate. Over many years, people have developed microfluidic devices for cell counting, which could provide a portable and economical solution to the problem.

1.2. Flow Cytometry

The medical standard currently used in hospitals and other research labs is flow cytometry, which is used to perform the cell counting, especially CBC. In this technique, cells are labeled with the antibodies raised for the specific antigen expressed on the desired cells surfaces. These antibodies are conjugated with fluorescent molecules called fluorophore. When excited by a certain wavelength the fluorophore is excited to a higher energy level. When a molecule absorbs a quantum of light, the valence electron moves to the higher energy (excited) state. The electron relaxes back to the lower orbit, i.e. the ground state, and releases the energy. Absorption occurs only at those wavelengths of light whose energy is equivalent to the energy difference in between the excited and the ground states. The wavelength at which the fluorophore gets excited is called its excitation spectrum. It relaxes to the ground state, emitting a radiation. The emitted light has a longer wavelength, and thus less energy, than the absorbed radiation.

After labeling the cells, they are made to pass through the flow cell in a single-file manner, where the laser excites the fluorophores attached to the antibodies on the cells as shown in Figure 1. The emitted light is detected by the different photodetectors. By detecting the forward scattered light, cells can be differentiated based on their sizes. However, by detecting the side scattered light, cells can be differentiated based on their internal cell structure and properties. Different emission filters are placed in front of a series of photodetectors to detect the specific emission wavelength. By getting the scatter plots of forward scatter vs. side scatter and selecting the appropriate gating, the cells can be counted [2].

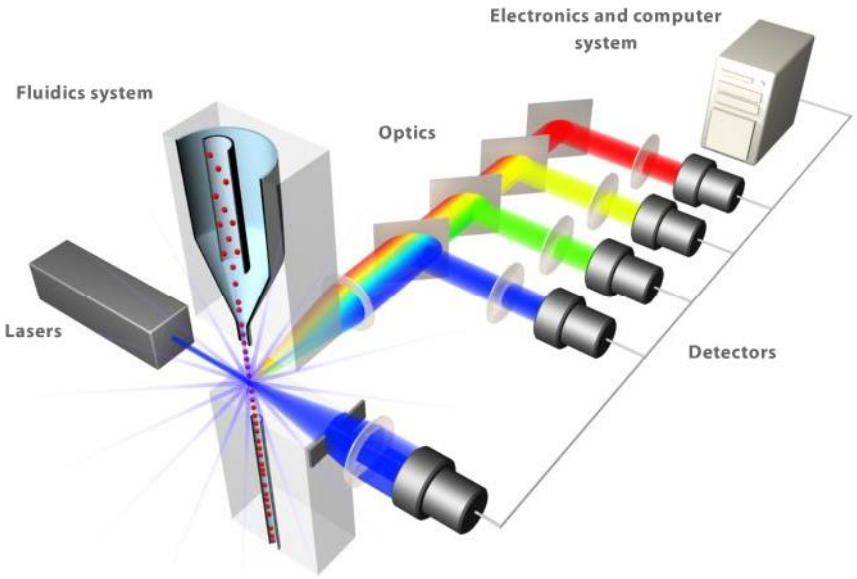

Figure 1: Internal schematic of the flow cytometer. The fluorophores on cells gets excited by the laser, and emitted radiation is detected by photodetectors. Adapted from [2].

1.2.1. Drawbacks

Although the flow cytometer gives accurate results, it is still not suitable for point of care settings in resource-limited regions of the world like sub-Sharan Africa due to the following reasons:

- The equipment is very expensive. The price varies from $50k to over $125k [3].
- Maintenance costs around $10k annually [3].
- The equipment is bulky (>50lbs).
- Trained technicians are required to operate this equipment and they are more difficult to find and train in resource-limited settings.

This clearly shows the need to have a portable, economical, and robust device for cell counting in resource poor regions.

1.3. Coulter Counting Principle

The Coulter counting principle was first presented by Wallace H. Coulter and was patented in 1953 [4]. Figure 2 shows how the Coulter counter works [5]. The chamber is filled with electrolytic solution. The metal electrodes are excited with a DC voltage. The particles/cells are made to pass one at a time through the small sensing aperture. While passing through that aperture the cells displace the electrolytic solution equal to their volume and increase the impedance of that region. The aperture is made smaller to restrict the electric field for better sensitivity. The change in the impedance is given by the equation 1.1.

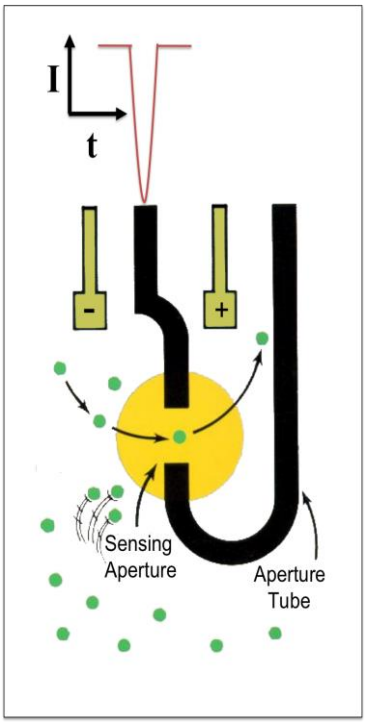

Figure 2: Coulter counting working principle. The passage of the non-conducting particle through the small aperture increases the impedance of the aperture cross-section [5].

$$\Delta R = 2\rho_{sol}\left(\frac{\arctan\left(r_p / \sqrt{\frac{A_c}{\pi} - r_p^2}\right)}{\pi\sqrt{\frac{A_c}{\pi} - r_p^2}} - \frac{r_p}{A_c}\right) \quad (1.1)$$

where A_c is the aperture cross-section, r_p is the radius of the particle and ρ_{sol} is the conductivity of the solution [6]. With the increase in the size of the particle and reduced aperture cross-section, the change in the impedance is higher.

If the particle is more conductive than the electrolytic solution, the impedance decreases, but if it is less conductive, the impedance increases. With the increase in the impedance, the current drops and downward pulses are obtained as the cells pass through the aperture. The depth of the pulse depends on the size of the particle; bigger particles displace more conductive solution and thus increase the impedance even more. For each passage of the cell, a pulse is produced. Thus, by counting all the pulses, one can find the concentration of the particles. And by determining the depth of the pulses the different size distributions of the particles can be isolated.

1.3.1. Effect of the coincident particles

For accurate counting of the cells, no two particles should pass through the aperture at one time. As shown in Figure 3(a), if two particles are widely spaced enough that for each passage of a cell a single unique pulse is obtained, then the particles can be accurately counted [5]. However if two particles are sufficiently close together they can pass through the aperture at the same time as shown in Figure 3(b) and for the optimum selected threshold can be counted as a single particle. Now, if two particles are combined

together as shown in Figure 3(c), they are together represented as a bigger size particle, resulting in a higher impedance of the aperture and resulting in a single pulse with a higher peak, thus counting as one particle.

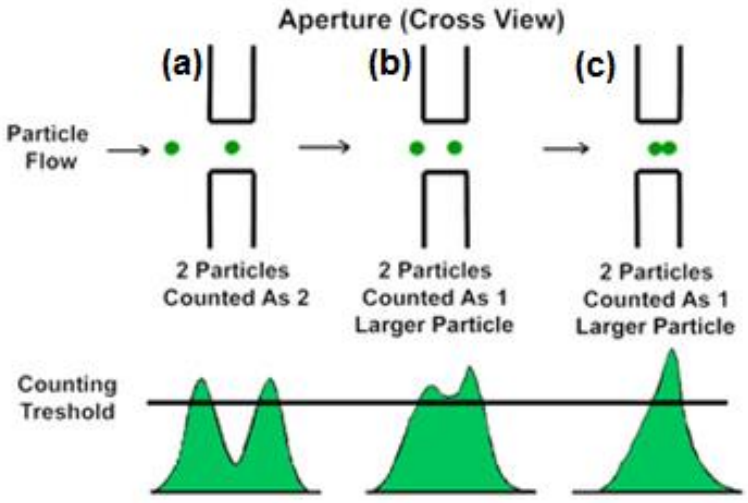

Figure 3: Effect of coincident particles on the detection and counting. Adapted from [5].

1.4. Electrical Counting of Cells

Cells respond differently to the application of the electric field. The response depends on the amplitude and frequency of the input signals.

1.4.1. Transmembrane voltage of a cell

Figure 4 shows the cell membrane and its intracellular and extracellular environment [7]. The plasma membrane of the cell is made up of a lipid bilayer which consists of phospholipid molecules whose heads are hydrophilic and tails are fatty acid chains (hydrophobic). When placed in aqueous medium, they form a lipid bilayer membrane.

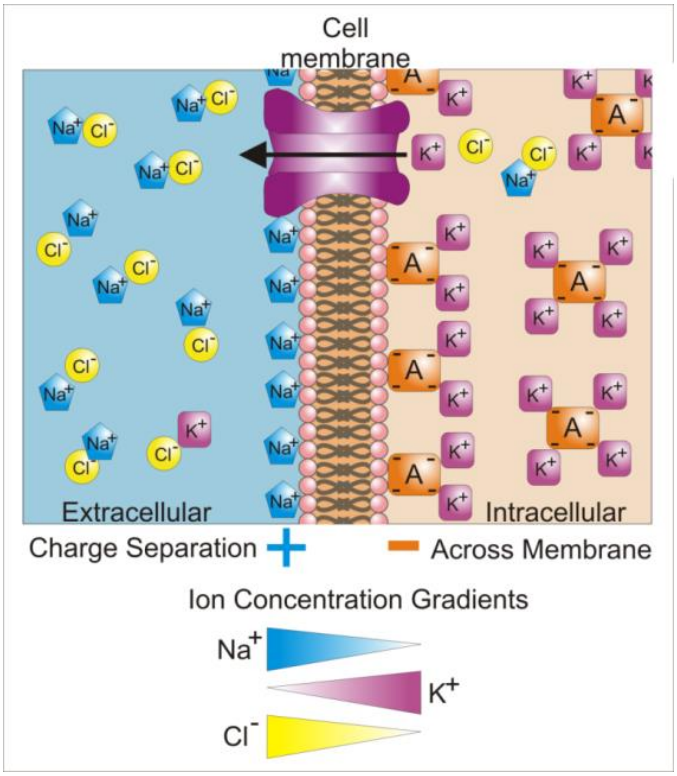

Figure 4: The cell membrane with its intracellular and extra cellular environment. The arrow shows the transport of K+ ions through the ion channel [7].

The cell membrane is highly permeable to the water molecules. However, it is highly resistive to any transfer of ions across the cell membrane. The concentration of the K+ ions inside the cell is higher as compared to outside. The concentration of the Na+ ions is lower inside than outside. The transfer of ions is only possible by activating the transmembrane proteins called ion channels. The concentration gradient of the K+ ions provides the necessary potential energy to activate the K+ ion channel which results in transfer of ions from intracellular to extracellular. This results in the negative charge inside the cell membrane and induces the positive charge outside the cell membrane. This potential difference across the cell membrane is called the transmembrane potential and its typical value lies in between -40 to -70 mV.

1.4.2. Electrical model of a cell

Figure 5 shows the electrical model of the cell [8]. R_s and C_s are the capacitance and resistance of the fluid surrounding the cell. R_{c1} and R_{c3} are the resistances of the plasma membrane (100MΩ), which is highly resistive to the flow of charges. C_{m1} and C_{m2} are the capacitances of the plasma membrane. R_{c2} is the resistance of the cytoplasm which comes in contact with the nucleus with nucleoplasm resistance, R_m. The capacitance of the nuclear membrane is represented by C_{n1} and C_{n2} and is approximately half of the membrane capacitance, since it is composed to two lipid bilayers [8].

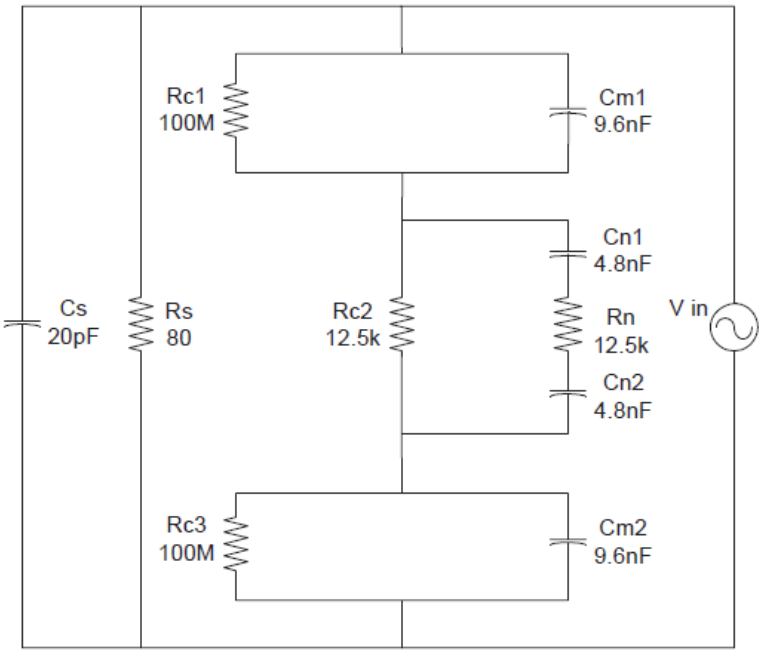

Figure 5: The equivalent electrical model of a cell suspended in the fluid [8].

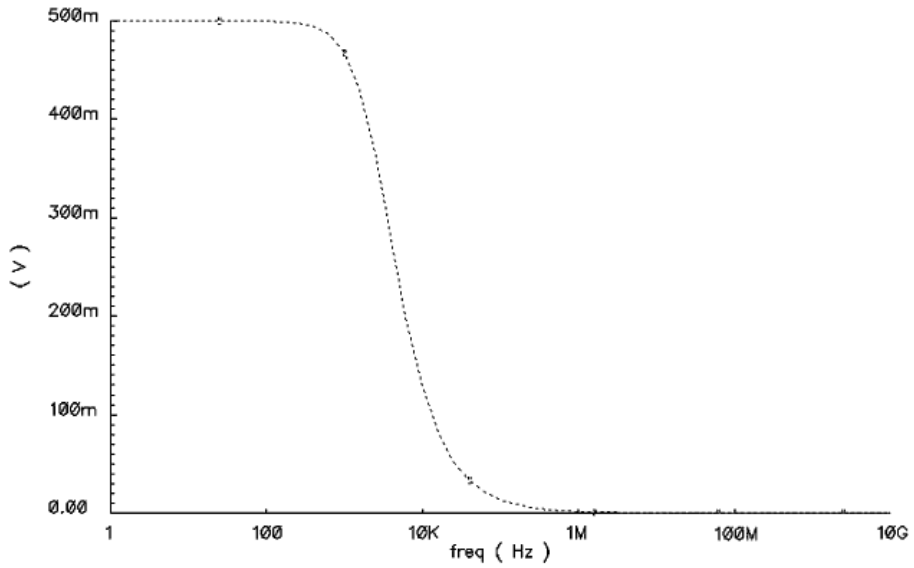

Figure 6: The voltage across the cell membrane with varying frequency [8].

Figure 6 shows the frequency response across the outer cell membrane. At low frequencies the input voltage appears at the plasma membrane, due to the plasma membrane resistance. At frequencies lower than about 100 kHz, the impedance change is based on the cell size, since at these frequencies cells behave as a non-conducting fluid [9]. At frequencies greater than 1 MHz, the change in impedance is based on different structural properties of the plasma membrane. At frequencies higher than 100MHz, the change in impedance is based on the nuclear membrane properties as shown in Figure 7. Thus, cells can be differentiated based on their sizes, plasma membrane and nuclear membrane structures.

Figure 8 shows the passage of the cell in a microfluidic channel and its equivalent electrical model. Below characteristic frequency of 1 MHz the impedance change is dependent on the cell size; however, at higher frequencies of greater than 1 MHz, the change in signal is dependent on the membrane characteristics. At further higher frequencies cytoplasm resistance plays the differentiation role.

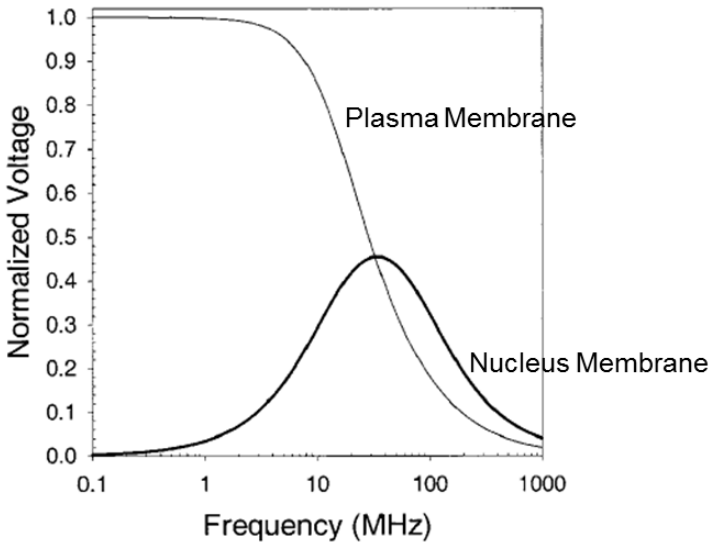

Figure 7: The potential drop across the plasma membrane (thin line) and nuclear membrane (thick line) with varying frequency [9].

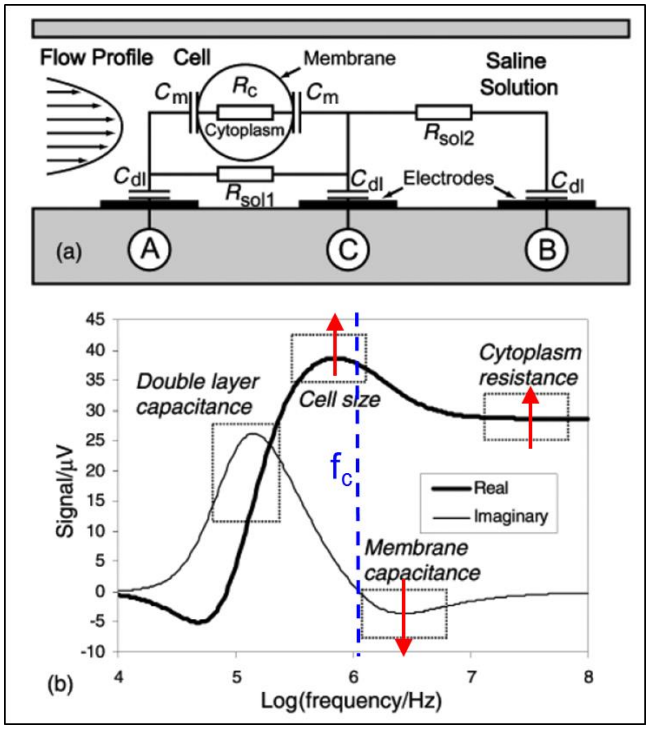

Figure 8: (a) The equivalent model of a cell when placed in conducting fluid. (b) Simulated impedance change with varying frequency [10].

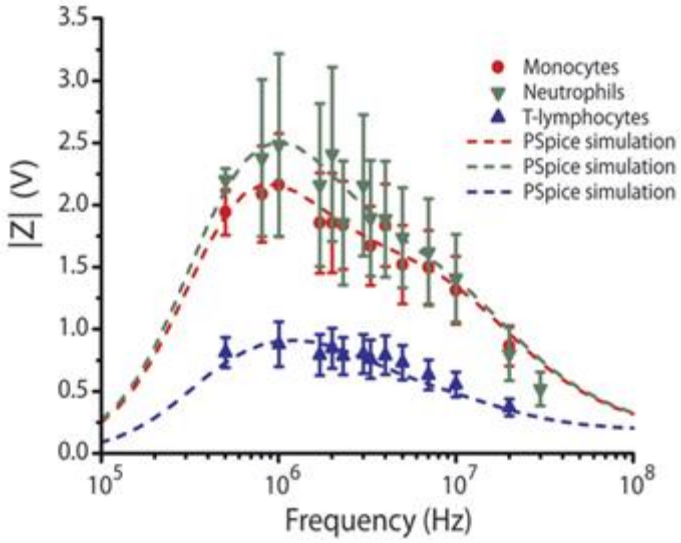

Figure 9: The simulated impedance change with frequency for different cell types. At lower frequencies the cells can be differentiated based on size, and at high frequencies around 1 MHz, the cells can be differentiated based on plasma membrane characteristics [10].

Figure 9 shows the simulation results of the impedance change. At frequencies of 100 kHz the lymphocytes can be distinguished from monocytes and neutrophils based on their size [10]. However, at higher frequencies of greater than 1 MHz the monocytes and neutrophils can also be differentiated from each other, as neutrophils have more folded membranes.

1.4.3. Electrical double layer capacitance

For a negatively charged electrode immersed in electrolytic solution, the partial positive H of the water molecule gets adsorbed onto the surface forming the first layer, called the stern layer. The second layer is composed of free ions attracted towards the stern layer by the Coulomb force; however, they are not anchored and can move freely because of thermal motion and electrostatic attraction. This layer is called the “diffuse layer” as

shown in Figure 10. Electric potential at the surface with respect to the bulk fluid is called the “electric surface potential” [11].

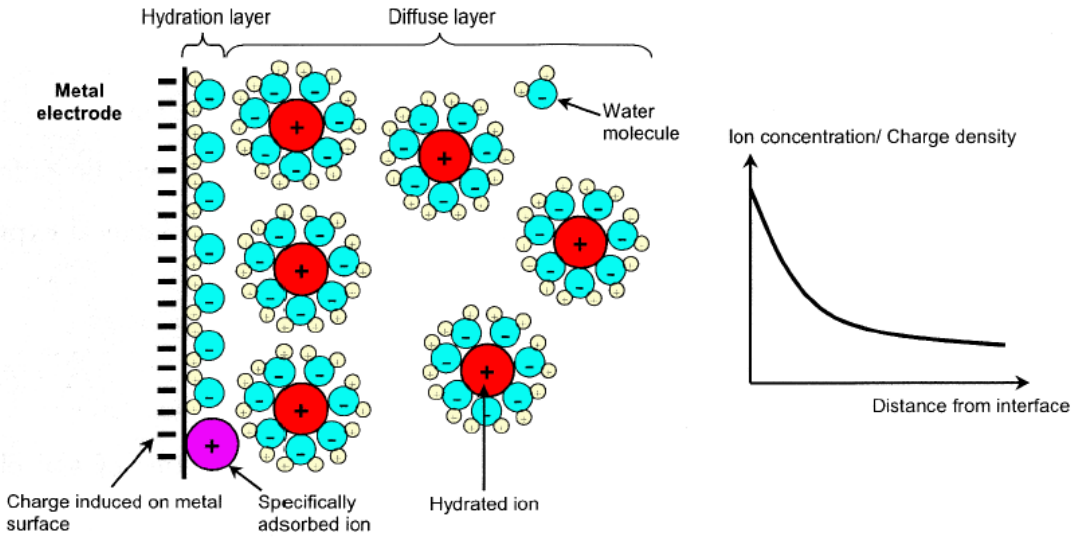

Figure 10: The formation of electrical double layer. The Debye length decreases with the increase in the distance from the interface [12].

The characteristic thickness of the double layer is referred to as the Debye length, which is inversely proportional to the square root of the ion concentration. In aqueous media its typical value is of the order of few nanometers.

1.5. Forces on a Particle in a Microfluidic Flow

A cell flowing in a microfluidic channel with electrodes experiences different forces, which are depicted in Figure 11.

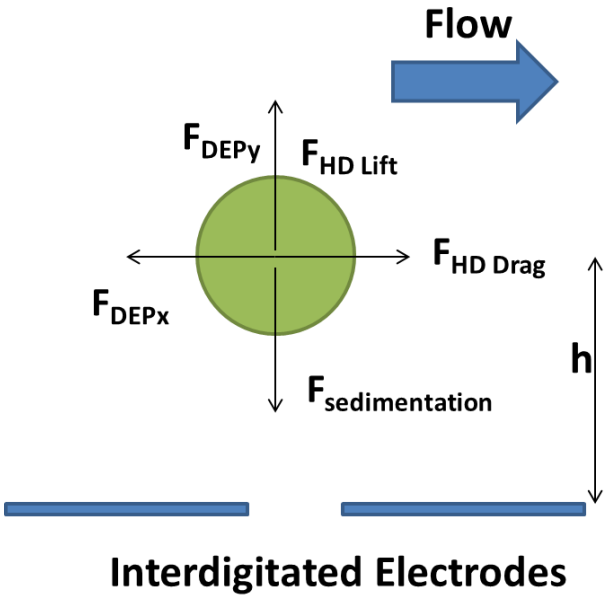

Figure 11: Effect of the different forces on the particle flowing in the fluid in the presence of electric field from interdigitated electrodes.

1. **Sedimentation Force**

   Sedimentation is the tendency of the particle to settle down in the fluid. It depends on the value of *g*, difference in conductivity between particle and medium and the size of the particle. For smaller sized particles, e.g. cells, this force is negligible [12]. It is given by Equation 1.2.

$$F_{sedi} = \frac{4}{3}\pi R^3 \left(\rho_p - \rho_m\right) g \tag{1.2}$$

2. **Hydrodynamic Drag Force**

   Particles suspended in the fluid experience a hydrodynamic force that depends on the relative velocity of the fluid with respect to the particle, co-efficient of viscosity and size of the particle [13]. It is given by Equation 1.3.

$$F_{HD-Drag} \approx 6\pi kR\eta\left(\upsilon_m - \upsilon_p\right) \tag{1.3}$$

For assuming a parabolic laminar flow profile,

$$\upsilon = 6\langle\upsilon\rangle \frac{x}{h}\left(1-\frac{x}{h}\right) \tag{1.4}$$

$$\langle\upsilon\rangle = \frac{U}{wh} \tag{1.5}$$

where U is flow rate in μL/min.

3. Hydrodynamic lifting force

Hydrodynamic lifting force tries to lift the particle in the suspension fluid and depends on the square of the size of the particle and co-efficient of viscosity. It is two orders of magnitude smaller than the typical DEP lifting force and can be easily neglected [13].

$$F_{HD-lift} \approx 0.153R^2\eta \frac{1}{(x-R)} \frac{d\upsilon_m}{dx}\Big|_{x=0} \tag{1.6}$$

4. Dielectrophoresis

A polarizable particle in the presence of a non-uniform electric field polarizes, and a force is produced, known as dielectrophoresis as shown in Figure 12. The non-uniform electric field exerts a force upon each end of the polarized particle; the mobility of the particle and its direction are determined by the difference in the magnitude of the two forces on each end [14]. DEP affects neutral particles and works for both DC and AC excitation. Positive DEP, movement of the particle in the direction of increasing electric field strength, occurs when the permittivity of the particle (ε_p) is greater than that of the medium (ε_m). Negative DEP occurs when $\varepsilon_p < \varepsilon_m$.

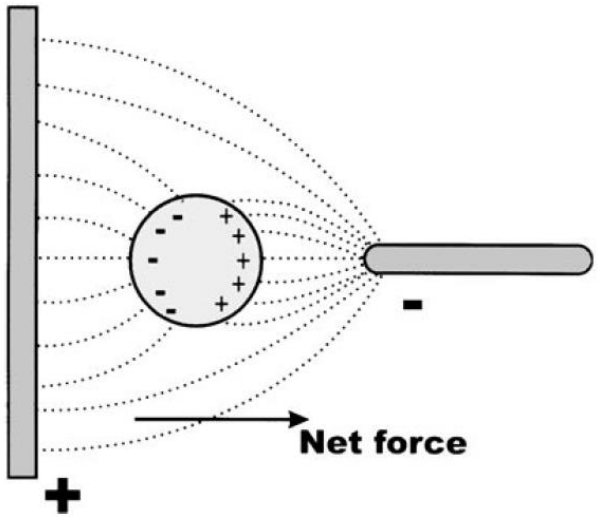

Figure 12: A polarizable particle in the presence of a point–plane electrode system. With application of electric field, the particle polarizes, and a force is produced. This effect is known as dielectrophoresis [15].

The DEP force depends on the size of the particle, permittivity of the particle (ε_p), permittivity of the medium (ε_m), electric field strength, real part of the Clausius-Mossoti factor f_{cm}. DEP force can be expressed by Equation 1.7.

$$F = 2\pi\varepsilon_0\varepsilon_m r^3 \,\mathrm{Re}[f_{cm}]\nabla |E_{RMS}|^2 \tag{1.7}$$

The Clausius-Mossoti factor f_{cm} is

$$f_{CM}\left(\varepsilon_p, \varepsilon_m\right) = \frac{\varepsilon_p - \varepsilon_m}{\varepsilon_p + 2\varepsilon_m} \tag{1.8}$$

The permittivity of the particle and the medium in Equations 1.7 and 1.8 are complex permittivity, which is a function of frequency:

$$\varepsilon_p = \varepsilon(\omega). \tag{1.9}$$

CHAPTER 2

ELECTRICAL COUNTING OF SPECIFIC WHITE BLOOD CELLS

2.1. Microfluidics and Lab-on-a-Chip

A microfluidic device can provide a solution to develop a point-of-care cell counting sensor. Such a device will start with a finger prick of blood, which directly goes to the chip, eliminating the need for off-chip sample preparation, and then a measurement module will provide the number of different types of blood cells.

2.1.1. Key criteria

The key criteria of a point-of-care cell counter include the following:

- It should use the least possible number of reagents for the whole assay, which effectively makes the procedure more economical.
- The device should take whole blood as input, eliminating the need for off-chip sample preparation and effectively reducing the assay time as well.
- The device should be economical for resource-limited settings. The cost per test should be reduced to $10 or less.
- The total assay time should be around 10-15 minutes or less.

2.2. Composition of Human Blood

Human blood is 55% plasma [16] and 45% platelets, white blood cells (also called leukocytes) and red blood cells (erythrocytes) as shown in Table 1. In each microliter of blood, there are almost 5 million erythrocytes and only 7500 leukocytes. Table 1 shows the different types of the blood cells, their properties and functions. The challenge lies in counting these few thousand cells out of millions of total cells.

2.3. Experimental Approach

The experimental flow of our cell counter is shown in Figure 13. The whole blood is infused on the chip where erythrocytes get lysed and then the white blood cells are counted using the microfabricated electrodes [17].

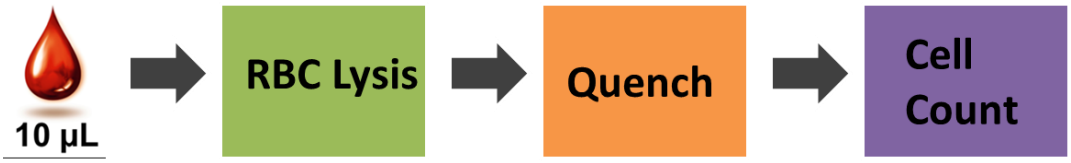

Figure 13: The process flow for the cell counting.

2.3.1. Cell counting approach

Figure 14 shows the approach for cell counting. Whole blood (10µL) is infused into one port of the device while from the other port the lysing reagent composed of saponin and formic acid (0.12% (v/v) formic acid and 0.05% (w/v) Saponin in DI solution) is introduced. This solution makes the surrounding medium for erythrocytes more hypotonic, thereby increasing the net inward osmotic pressure difference, resulting in lysing of the red blood cells. The lysing time was optimized to completely lyse all the

Table 1: The different types of cells found in blood with their functions, concentration and size.

Cell Type	Function	Concentration #/μL	Size (Diameter) μm
Erythrocytes (RBC's)	O_2 and CO_2 transport	$5x10^6$	6-8
Thrombocytes (Platelets)	Blood clotting	$3x10^5$	2-3
Leukocytes (WBC's)	Immune defense	$4\text{-}11x10^3$	7-21
Neutrophils	Kill invading bacteria	$5x10^3$	10-12
Eosinophils	Modulate allergic inflammatory responses	$2x10^2$	10-12
Basophils	Histamine release for immune responses	$4x10^1$	12-15
Monocytes	Differentiate into dendritic cells	$4x10^2$	14-17
Lymphocytes		$3x10^3$	7-8
B Cells	Make antibodies	$2x10^3$	7-8
T cells	Kill virus infected cells and regulate other leukocyte activities	$1x10^3$	7-8
Natural Killer cells	Kill virus infected and some tumor cells	$1x10^2$	7-8

red blood cells. The quenching buffer is then infused from the third port and is composed of sodium carbonate and PBS. The main objective of this solution is to halt the lysing process and maintain the pH of the solution [17]. The remaining leukocytes pass through the set of microfabricated electrodes which count all the passing cells and provide the cell counts. By probing the cells at different frequencies, the different types of white blood cells can be differentiated based on their size, and cell membrane morphology. Figure 15 shows the schematic of the device with different regions where the respective processes take place.

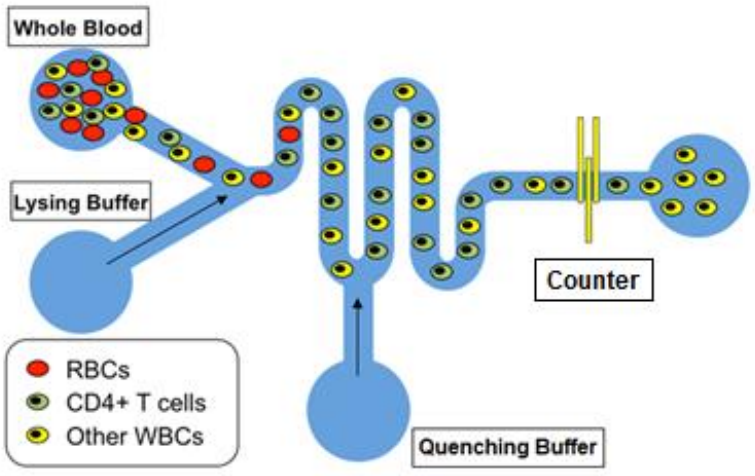

Figure 14: The schematic of the cell counting approach. The whole blood is lysed with lysing buffer and then the quenching buffer is infused to halt the lysing and maintain the osmolarity.

2.4. Electrical Counting of Cells

Much progress has been made in impedance microcytometry with alternating current interrogation to detect differences in chemically modified cells [18], to evaluate cellular

processes [19], and discriminate among cell types [20, 21]. The technique still has not proven to be sensitive enough to distinguish among cells that have similar morphologies, such as CD4+ T lymphocytes and other lymphocytes.

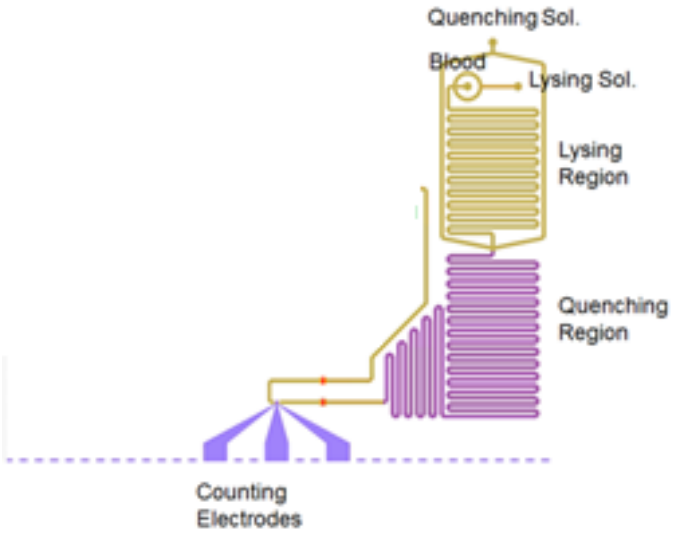

Figure 15: The schematic of the device showing the ports where samples are infused. Lysing region, quenching region, and electrodes are also represented.

Figure 16(a) shows the microfabricated electrodes. The yellow arrows show the typical cells passing through the chamber. The counting channel has a cross-section of 15 x 15μm^2 which facilitates the signal strength [22]. For each passage of the cell, the electrodes generate a bipolar pulse as shown in the enlarged version of Figure 16(b). At the counter, all these pulses are counted to obtain the total count by selecting the appropriate threshold.

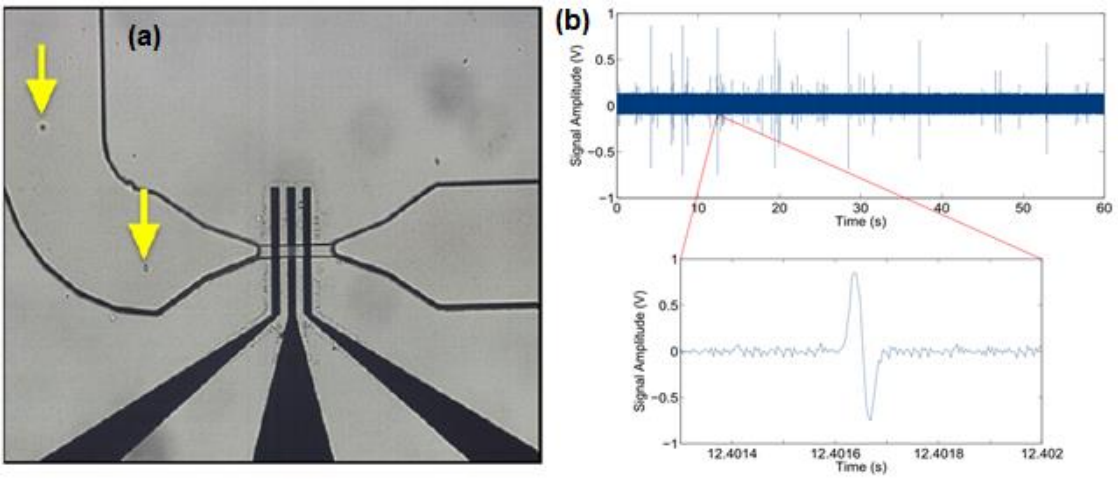

Figure 16: (a) Micro fabricated electrodes. The yellow arrows show the typical cells flowing. (b) The pulses it generates with the passage of the cells [22].

2.4.1. Analysis of counts

The lock-in amplifier injects 303 kHz and 1.7 MHz signal to the middle counting electrode. Relative impedance is measured by a Wheatstone bridge circuit. At low frequencies like 303 kHz, the leukocytes can be differentiated based on the cell size. At this frequency, the cells act as non-conducting spheres and completely block the electrical current when they displace the conductive fluid which depends on the size/ volume of the cell. The histogram at 303 kHz is shown in Figure 17(a) in which lymphocytes are easily distinguishable from monocytes and granulocytes. At high frequencies around 1.7 MHz, the measured impedance depends upon the cell membrane capacitance and cell morphology. For example, monocytes have higher cell membrane capacitance and have extensive folding in the membrane as compared to neutrophils, so they can be differentiated. Thus, by probing the cells at these frequencies we can differentiate between erythrocytes debris and different types of leukocytes like

lymphocytes with granulocytes and monocytes. Figure 17(b) shows the scatter plot of opacity (which is the impedance change due to high frequency divided by the impedance change due to low frequency) versus the impedance change at low frequency (303 kHz). As shown in the figure, we can easily distinguish the red blood cells debris and the two cell distributions show the differentiation between lymphocytes and granulocytes [22]. The dashed rectangular gates are drawn and cells enclosed in the gates were counted as forward and reverse counts respectively.

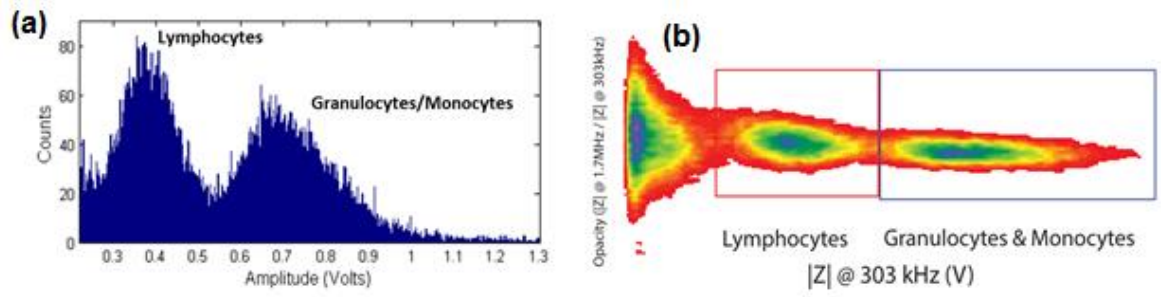

Figure 17: The low frequency histogram distribution [23]. (b) The opacity vs. low frequency scatter plot. Lymphocytes can easily be differentiated from monocytes and granulocytes. A gating technique was used to determine the total leukocyte and lymphocyte counts [22].

2.5. Validation of Electrical Counts (Comparison with Optical Counts)

To check the accuracy of the electrical counting procedure, the electrical counts are compared with the optical counts. After the lysing, quenching and forward counting of the blood, the sample is collected into the tube filled with 1200μL of PBS+1%BSA, and then it is centrifuged for 5 min at 300rcf; supernatant is poured out and the cell pallet is further mixed in 600μL of PBS+1%BSA. This sample is run through a flow cytometer to

count the total number of cells present [22]. Figure 18 shows a high correlation, with an R^2 value of 0.9584, between total forward count from the chip and the optical count from the flow cytometer, thus proving the validity of the electrical counting measurement procedure.

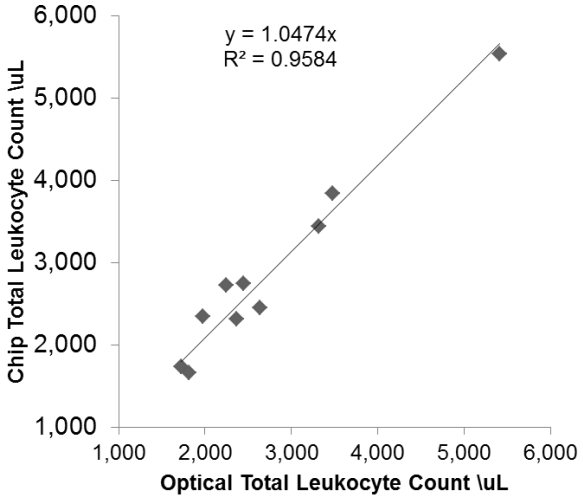

Figure 18: The comparison of the electrical chip counts vs. the optical counts obtained from flow cytometer. The R^2 value of 0.9584 shows the accuracy of the electrical counting method [22].

2.6. Cell Viability Analysis

The effect of the lysing and quenching buffers on the cell viability is investigated by counting the cells in two experimental approaches. In the first case, only one counter is used and the flow is reversed to get the second count. In the second case, two counters are used. Both the approaches are discussed in the following.

2.6.1. Single counter approach

In order to capture specific cells, after the counter, they are passed through the capture chamber where the antibody for the specific cells to be captured is initially immobilized. With the optimized shear stress for maximum capture efficiency as the cells pass through the capture chamber, the desired cells get captured by the antibodies. The remaining cells are collected into the holding coil, and then flown back with the washing buffer, i.e. PBS, as shown by Figure 19. The cells pass through the same electrodes and provide the *reverse count*. By taking the difference in between the entrance and the reverse counts, the number of captured cells is calculated.

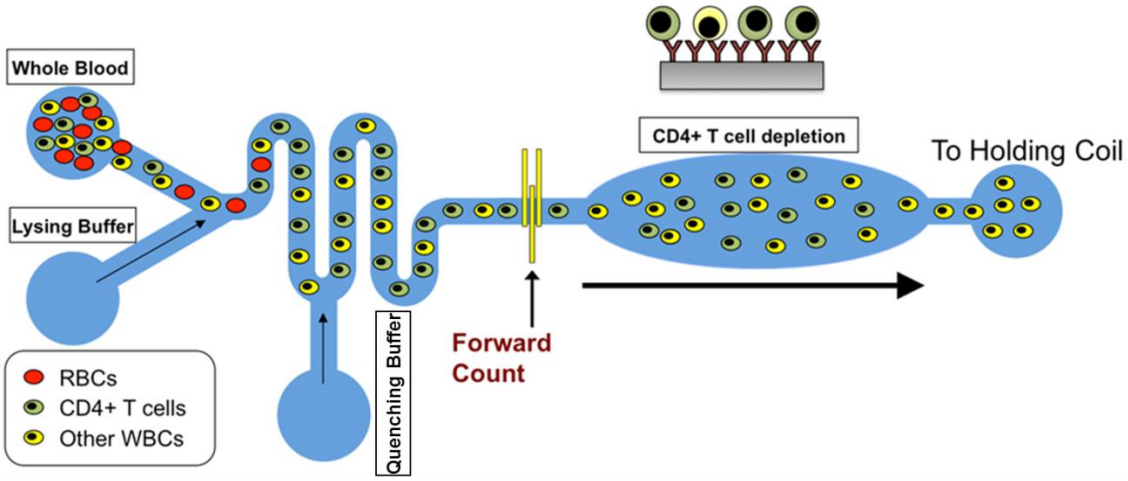

Figure 19: Schematic for the single counter approach. After lysing, quenching and forward counting, the cells are held in the holding coil before reversal. The cells are then counted again to get reverse count.

Another important characterization of the device is to check that the differential count between entrance and reverse count is zero if there is no capture chamber between the counters. Figure 20 shows the protocol for this study in which after entrance count,

the cells goes to the holding coil and then are reversed to flow back and provide the reverse count.

Figure 20: Protocol for cell vitality studies in single counter approach.

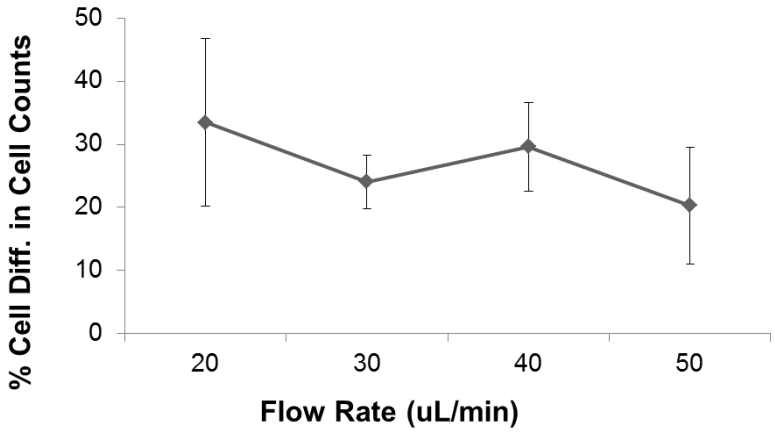

Figure 21: The percent cell count difference between forward flow and reverse flow at different flow rates is >30% [22].

Table 2: Total Experiment time vs. time of exposure of lysing and quenching buffers in case of a single counter.

Flow Rate (µL/min)	Single Counter Experiment Time (min)	Exposure to the lysing + quenching buffer (Single) (min)
20	45	30
30	35	25
40	30	22.5
50	23	17

Figure 21 shows the percent cell count difference in between the entrance and the reverse counts. The flow rate is varied from 20 μL/min to 50 μL/min and found to be 35% at 20 μL/min and almost 20% at 50 μL/min. The reason for such a huge difference can be attributed to the cell loss or cell death due to the prolonged exposure of the lysing and the quenching reagents. Table 2 shows the total experiment time and the time the cells get exposed to lysing and quenching buffers in the holding coil. For example, at 50 μL/min the total experiment time is 23 min, during 17 minutes of which cells remain in the holding coil and 20% of the cells die as compared to the 35% cell death at 20 μL/min, in which the cells remain in the holding coil for almost 30 min out of a total experiment time of 45 min [22].

2.6.2. Dual counter approach

The cell viability can be improved by reducing the exposure time of the lysing and quenching reagents to the cells. For this purpose another counter is introduced after the capture chamber as shown in Figure 22, thus providing the *exit count*. The capture chamber is replaced with tubing of equal volume (as of capture chamber), i.e. 15 μL. The protocol for the dual counter cell viability analysis is shown in Figure 23.

Figure 24 shows the percent cell count difference between the entrance and the exit counts. The flow rate is varied from 20 μL/min to 50 μL/min and found to be around 0.5%, which is a result of reduced exposure of lysing and quenching reagents to the cells. Table 3 shows the total experiment time and the time the cells get exposed to lysing and quenching buffers for the experiment. The exposure time has been reduced to less than a minute [22].

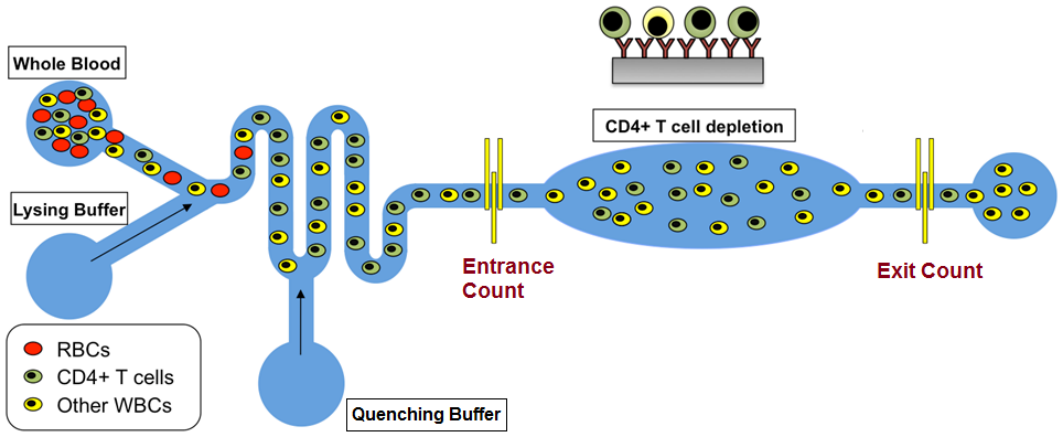

Figure 22: Schematic for the dual counter approach [23].

Figure 23: Protocol for cell vitality studies in dual counter approach. Tubing of 15µL is used in between the two counters.

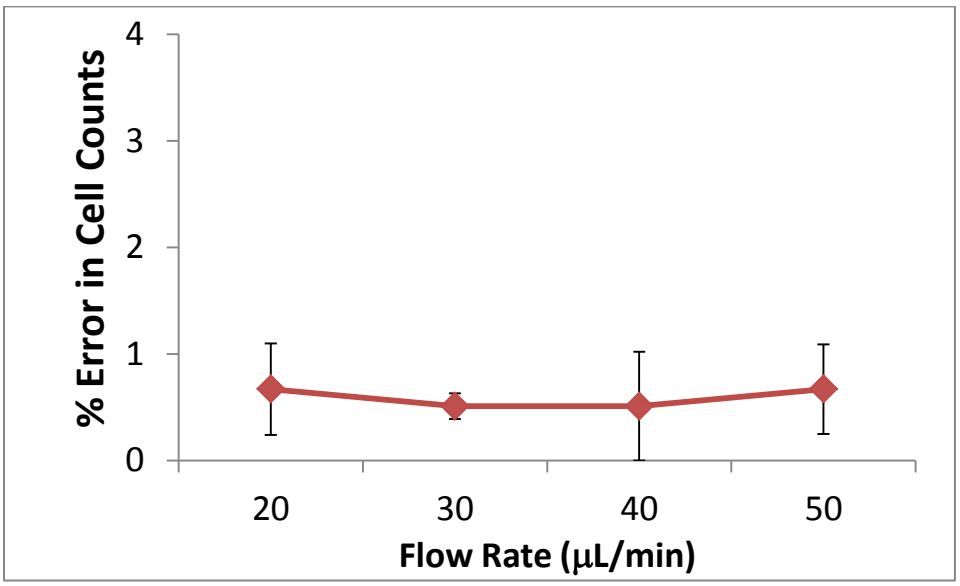

Figure 24: The percent cell count difference in between forward flow and reverse flow at different flow rates is around 0.5% [22].

Table 3: Total Experiment time vs. time of exposure of lysing and quenching buffers in case of a dual counter [22].

Flow Rate (μL/min)	Dual Counter Experiment Time (min)	Exposure to the lysing + quenching buffer (min)
20	20	0.75
30	15	0.5
40	13	0.375
50	10	0.3

2.7. Experimental Setup

Figure 25 shows the experimental setup. An Eksigent Nanoflow LC pump (Dublin, CA) is used to infuse the lysing, quenching, and PBS reagents into the chip at desired flow rates. A Rheodyne MHP7980-500-1 valve (Rohnert Park, CA) is used to load 10 μL of blood sample into a 10 μL holding coil (via syringe) and then direct PBS through the coil to inject the blood sample into the chip [22].

A Zurich Instruments (Zurich, Switzerland) HF2LI lock-in amplifier was used to simultaneously inject 303 kHz and 1.7 MHz AC signals of 5V rms into the chip's center counting electrode. Relative impedance was measured by creating a Wheatstone bridge circuit with 10 kΩ resistors [17]. The voltage difference between the two Wheatstone branches was fed to the differential preamplifier (Zurich Instruments). The signal is then fed to the lock-in amplifier and sampled at 250 kHz in LabVIEW on a computer with a

PCI-6351 DAQ card (National Instruments, Austin, TX). A customized Matlab program was developed to count the pulses at the user-desired threshold value (Appendix A).

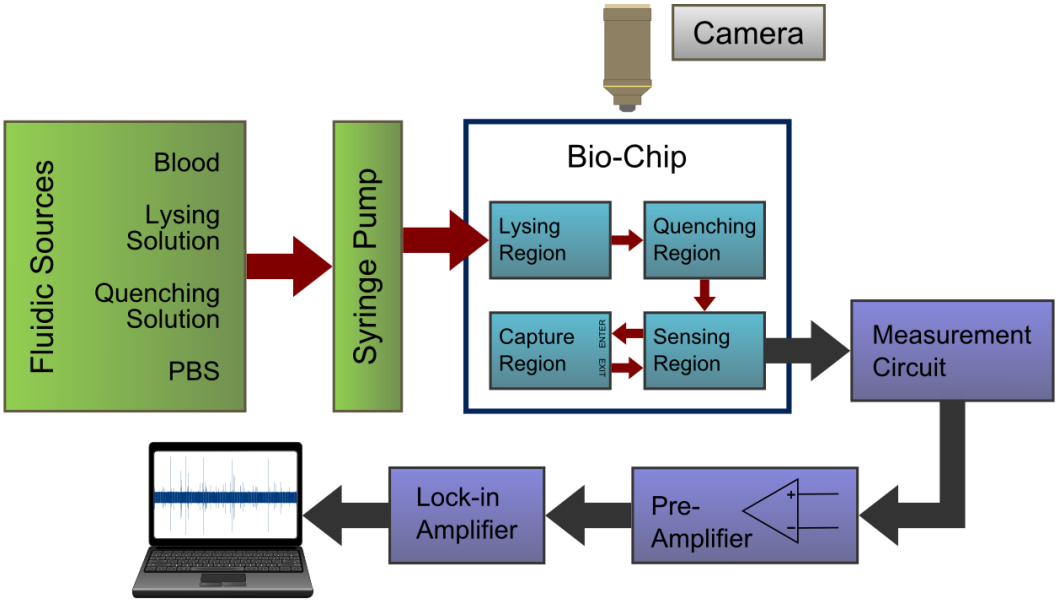

Figure 25: Schematic of the experimental setup [22].

2.8. Fabrication

2.8.1. Electrodes fabrication protocol

Electrodes were fabricated on a 4 inch Pyrex Glass wafer using the following protocol:

1. Piranha clean (sulfuric acid: hydrogen peroxide, 1:1) for 15 minutes and then rinse 10 times.

2. Dehydration bake is performed at 110 °C for 5 minutes minimum with 5 minutes cool-off time.

3. LOR 3A is spin-coated for 500 to 3000 rpm in 2 sec and hold for 35 sec.

4. Soft bake is done at 183 °C for 5 minutes with further 5 minutes cool-off time.

5. S1805 is spin-coated for 500 to 4000 rpm in 3 sec and hold for 40 sec.

6. Soft bake is done for 90 s at 110 °C with 5 minutes cool-off to prevent wafer from sticking to mask.

7. The wafer is exposed for 1.3 seconds; time is calculated based on the exposure energy and power output.

8. Post-exposure bake is done for one minute at 110 °C.

9. The wafer is developed in CD-26 for 20 s.

10. Before metal deposition the wafer is cleaned using oxygen plasma for 20 sec.

11. Metal evaporation is done for 250 Å of titanium and 750 Å of platinum.

12. Metal lift-off is done using Remover PG.

2.8.2. Fluidics mask fabrication

The multilevel fluidics layer was created using standard rapid microfluidic prototyping using Microchem SU-8 negative photoresists and Poly(dimethylsiloxane) (PDMS). A negative master was constructed on a 4" Si wafer using four successive iterations of the standard SU-8 recipe, with all soft-bake and post-exposure bake durations and temperatures being similar to those suggested in the SU-8 product sheets [22]. SU-8 was spun to a height of 15 µm and exposed using the EV420 mask aligner to define the counting and filter regions and provide a base for the other regions. A 55 µm layer was then spun on and exposed to define the 60 µm tall capture region. 30 µm of SU-8 50 was deposited to define the 100 µm lysis region, followed by a 50 µm layer to create the 150

μm quenching region. Development in SU-8 developer was deferred until all four layers were created. After development and rinsing the mold with IPA, a 1:10 curing agent to base mixture of PDMS was poured over it and cured for at least 15 minutes at 150 °C to create the fluidic channels. The fluidic inlets and outlet were cored out of the PDMS mold using a custom hole punch [22].

CHAPTER 3

FLOW METERING OF BLOOD IN A MICROFLUIDIC DEVICE

3.1. Introduction

The flow metering of the blood in a microfluidic device is reported. The flow metering is based on the measurement of the electrical admittance. The human blood is lysed and quenched in the microfluidic device and then flowed over the pair of electrodes. With the change in the flow rate the impedance signal changes. This chapter also shows the increase in the number of cells as the flow rate increases. The decrease in the pulse width and pulse amplitude with the increase in flow rate is also experimentally verified. The flow metering and the cell counting are done simultaneously.

The need of flow metering in a microfluidic device was reported a few decades ago when Putten [24] made the first silicon technology based flow sensor. The sensing mechanisms used are heat detection [25], atomic emission detection [26] and periodic flapping motion detection [27]. The heat sensing mechanism works by measuring the temperature difference in a microchannel between two points. Such sensors are complicated in design as they require the heating and heat sensing mechanisms on the same device [25].

3.2. Electrical Flow Metering

In microfluidic channels, the fluids flow in a parabolic profile under laminar conditions. For an electrolytic fluid, the ions in the middle of channel travel faster than those near the walls, resulting in the redistribution of ions within the electric double layer in the channel [28]. When the AC voltage is applied across the channel electrodes, the ions move backward and forward across electrodes. The electro-kinetic effects are developed because of ionic redistribution, which results in changing the electrical admittance. Thus, the flow of the fluid in a microchannel is related to the change in the admittance across the microelectrodes. The different parameters including the amplitude of AC voltage, the frequency of the signal, the conductivity of the electrolyte, and dimensions of the electrodes needs to be optimized for better sensitivity [28, 29]. With the increase in the flow rate the mass transport increases due to increase in the ionic concentration. Thus, the mass transport limited current is increased as it is directly proportional to the flow rate [28] and is given as

$$i_L = 0.925nF[A]_{bulk} D_A^{2/3} Q^{1/3} w \sqrt[3]{x_e^2 / h^2} \tag{3.1}$$

The equivalent circuit model is shown in Figure 26. The solution in channel offers parallel Rs and Cs impedance while electrodes offer series capacitance Ce. Ce is due to the free electrons on the electrode surface. Cs arises due to ion depletion or excess in the channel.

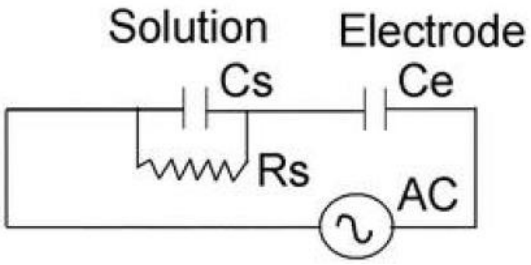

Figure 26: Equivalent circuit model for the flow metering in a microfluidic channel [30].

3.3. Flow Metering of Lysed Blood

Performing the flow metering in a microfluidic device with the human blood finds many applications in many diagnostic devices and accurate measurements of the cell concentrations per microliter of blood. Human blood has blood cells which are suspended in blood plasma, which is a fluid comprising 55% of blood and contains Glucose, proteins, and consists of ions including sodium, potassium, chloride, calcium, magnesium, phospahte, and sulphate [31]. The sodium and chloride ions are present in maximum concentration, which is around 140 and 100 mmol/l respectively.

3.3.1. Experimental method

In our microfluidic device, the 1 mL of blood is lysed by adding (0.12% (v/v) formic acid and 0.05% (w/v) saponin in DI). Lysing was then stopped by adding the quenching solution of (5.3 mL of 0.6% (w/v) sodium carbonate and 3% (w/v) sodium chloride in DI). Then, the suspension is done in PBS + BSA [32]. The lysing and the quenching regions on the device are shown in Figure 27.

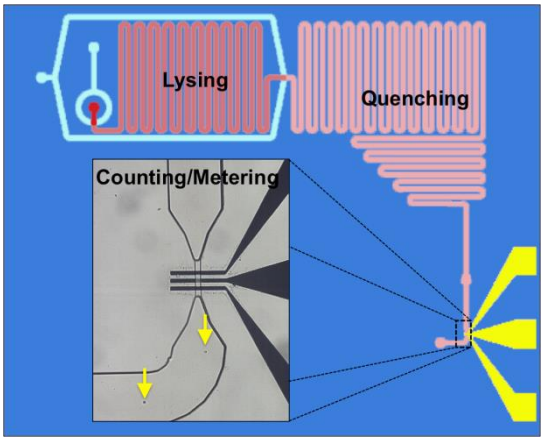

Figure 27: Schematic of the device with electrodes used for counting/metering [32].

The platinum electrodes were fabricated on a glass substrate. The 75nm of Pt conduction layer is deposited on a 25nm Ti adhesion layer. The electrodes are being used for counting the cells as they pass by. An AC signal of about 5 Volt and 500 kHz is applied to the electrodes [32]. We shall be using the same set of electrodes for the measurement of the flow rate as shown in Figure 28. The output signal from the electrodes is fed to the lock-in amplifier to obtain the output.

Initially, for the known set of flow rates, the current is measured to obtain the calibration curve for the flow sensing method. Then, it will be used in the real run-time experiment to find the actual flow rates.

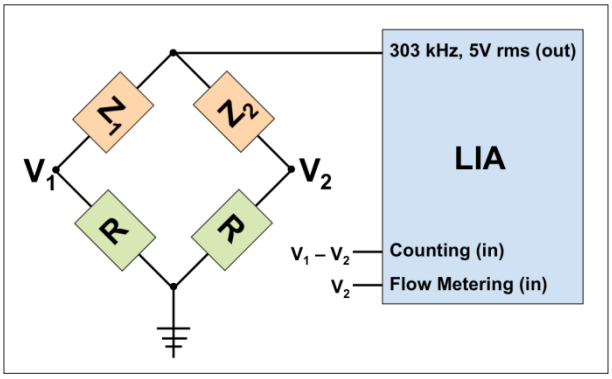

Figure 28: Electrodes setup used for counting the cells and metering the flow rate of lysed Blood [32].

3.4. Results

In our microfluidic device, as we increase the flow rate, the signal amplitude increases. To establish a background noise signal, we measure the signal amplitude while no fluid is flowing or the fluid is at rest. This gives us a background noise which we subtract from all of our subsequent readings for different flow rates. The background signal amplitude we have measured is -4.83 Volt. The flow rate is varied from 10 to 60 μL/min and the mean signal amplitude is measured and subtracted from the background noise. The results obtained are shown in Figure 29.

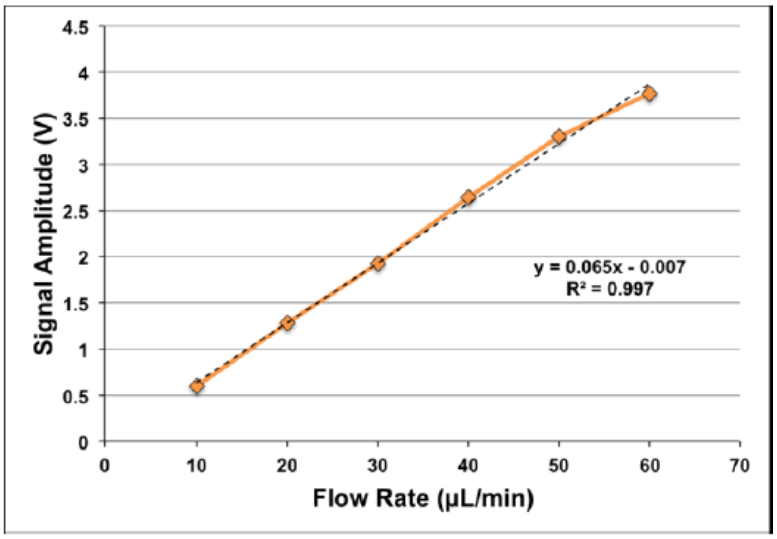

Figure 29: Linear increase in the signal amplitude with the flow rate. The mean value of the signal amplitude is taken [32].

3.4.1. Flow rate vs. cell counting

While the flow rate is being measured form one data acquisition channel, the second channel is used to obtain the data for the cell counting. We have used our custom built code to count the number of peaks above a certain threshold value. All such peaks

obtained shall be counted as cells. The threshold value can be selected in different ways, one of which is to take the 3-5 times the standard deviation of the signal. The threshold amplitude we selected is 0.02 V. As expected, with the increase in the flow rate the number of cells counted in a given time should be increased. This is clear from Figure 30. With the increase in flow rate the number of cells increases, but for higher flow rates we cannot see the anticipated increase in the number of cells because of the fact that the pulse amplitude also starts decreasing as the flow rate increases as shown in Figure 31.

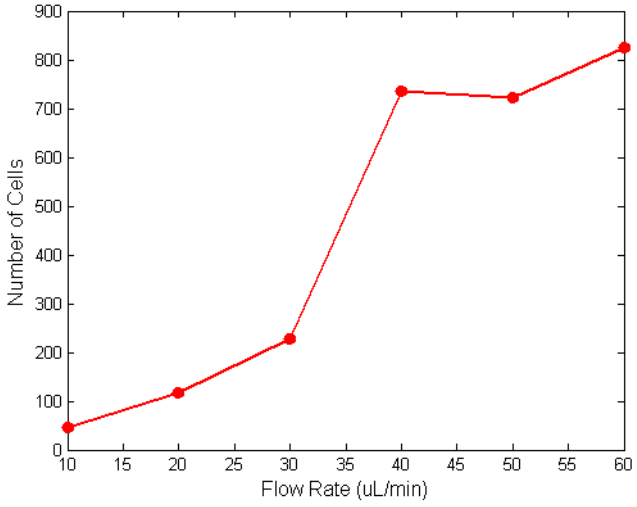

Figure 30: Increase in the number of the cells as the flow rate increases. With increased flow rate, more cells passes through a given point in some fixed time [32].

3.4.2. Flow rate measurement using pulse width

As we know, if the flow rate is increased, the detected signal's pulse should be reduced along with the pulse peak amplitude. This is shown in the Figure 32 in which it is clear that, as the flow rate is increased from 10-60 μL/min, pulse width has reduced from 11.6 μs to 3.4 μs. Similarly, the pulse amplitude has reduced from 0.01218 V to 0.0445 V [32].

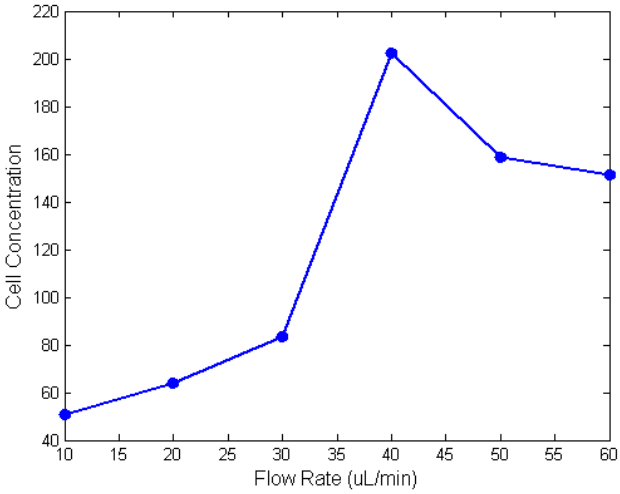

Figure 31: Cell concentration as the flow rate is increased [32].

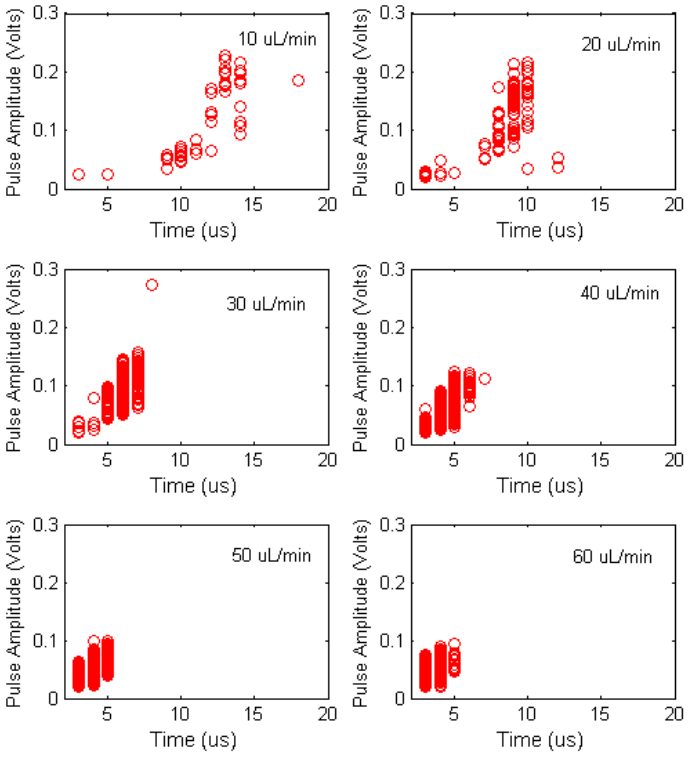

Figure 32: Pulse amplitude vs. pulse width time for different flow rates. With the increase in the flow rate the pulse amplitude decreases and the pulse width also decreases [32].

Figure 33 shows the decrease in the pulse width as the flow rate is increased. It also shows the standard deviation bars on the mean values. Another important observation is the decrease in the standard deviation with the increase in the flow rate. Figure 34 shows the decrease in the pulse amplitude as the flow rate increases. The standard deviation, in this case as well, decreased with the increase in flow rate.

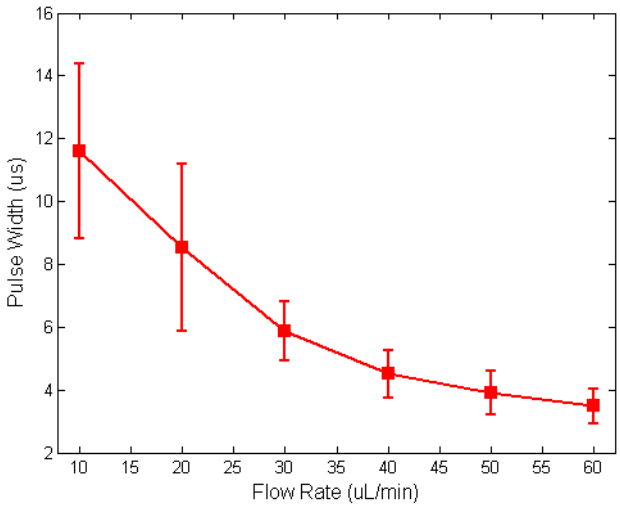

Figure 33: Decrease in the pulse width as the flow rate is increased [32].

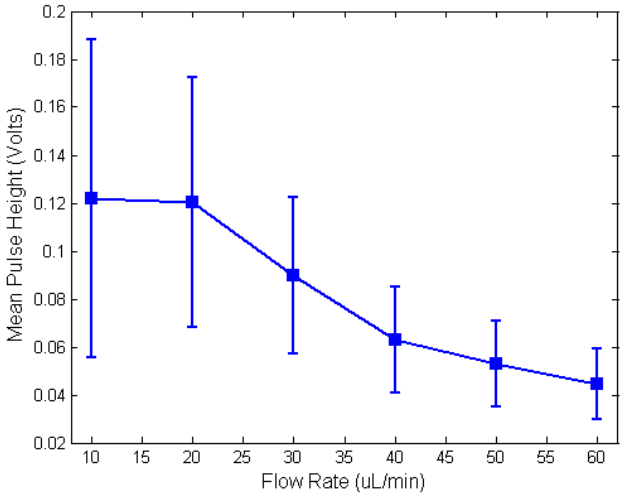

Figure 34: Decrease in the pulse amplitude as the flow rate is increased [32].

3.5. Conclusion

We have shown a flow metering in a microfluidic device with the lysed blood. The cells are counted simultaneously while metering the flow. The increase in the number of cells, the decrease in the pulse width and height, with the increase in the flow rate show the significance of monitoring the flow rate while doing other impedance measurements [32].

CHAPTER 4
FUTURE WORK

4.1. CD4 and CD8 T Cell Counter with Flow Metering

The differential counter can be used for counting any specific white blood cells. There are 34 million people infected with HIV/AIDS worldwide with the lack of testing facilities in resource-limited settings [33]. The most important diagnostics biomarker for HIV/AIDS is the absolute count of the CD4+ and CD8+ T lymphocytes in the whole blood [34]. Current standard practice for CD4+/CD8+ cell counting uses flow cytometry that is readily available in developed nations but unavailable in underdeveloped regions due to limited resources and lack of technical personnel to maintain and operate these equipment. Therefore, a lot of effort has been put into developing inexpensive and portable CD4+, CD8+ T cell counters that would bring the test to the point-of-care settings in resource-limited regions of the world [34, 35]. AC impedance analysis with microfabricated electrodes can be used to electrically interrogate and count the cells. The differential counting technique is based on effectively lysing the erythrocytes and counting the remaining leukocytes before and after capturing the selective CD4 or CD8 T cells [19, 20].

The highest possible capture efficiency can be ensured in the following ways:

- Different surface chemistries, physio-adsorption vs. covalent based surface chemistry.

- Design of the capture chamber. Planar capture chamber allows the Abs to bind only at the surfaces. However the capture chamber with pillars can increase the surface area for maximum capture efficiency.
- Optimization of the shear stress. Shear stress depends on the dimensions of the chamber, its height and width. It also depends on the flow rate of the fluid. By optimizing all these factors the optimized shear stress for maximum capture efficiency can be found.

This device shown in Figure 35 can also perform flow metering of whole blood. This eliminates the need of manually monitoring of the 10 μL of blood for infusing into the device.

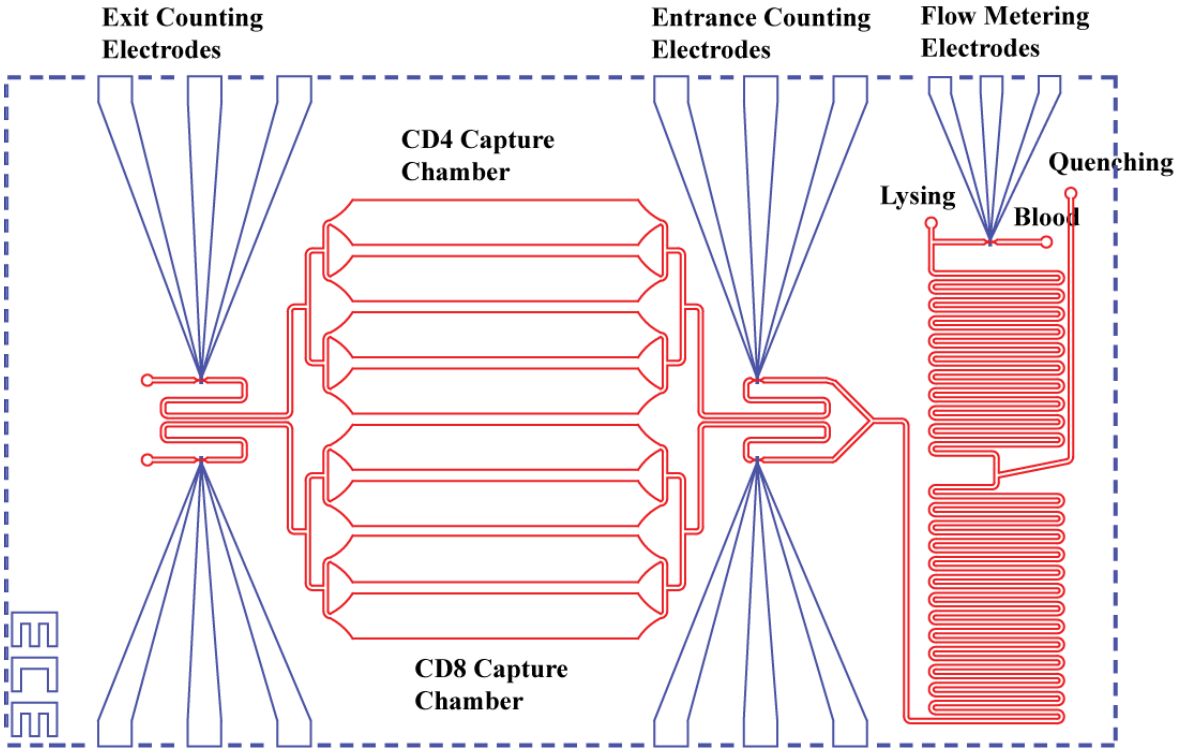

Figure 35: CD4 and CD8 T cell counter with blood flow metering for HIV/AIDS diagnostics.

4.2. Complete Blood Cell Count

The complete blood count (CBC) is among the most ubiquitous diagnostic tests in primary care. CBC would be highly useful in Acute Radiation Syndrome (ARS) where immediate CBC with differential is required for its rapid management of the disease. In chemotherapy and radiation therapy, the blood cell production needs to be monitored by a CBC. Inflammation, leukemia, tissue injury, bone marrow failure and immunodeficiency can be identified by the irregular WBC counts and their differentials. Similarly, bone marrow fibrosis, lymphoma, aplastic anemia and lupus erythematosus are associated with abnormal platelet count. Excessive bleeding, kidney bleeding, cancer and mechanical trauma can be identified by the RBC count. Thus, a microfluidic, disposable, economical CBC would help in monitoring all these diseases with more efficiency and care [1]. Most of the commercially available machines are based on flow cytometry and Coulter detection principles [36].

The differential counting approach can help in designing a microfluidic CBC which provides the erythrocyte, platelet, and white blood cell differential count. The concept is shown in the Figure 36.

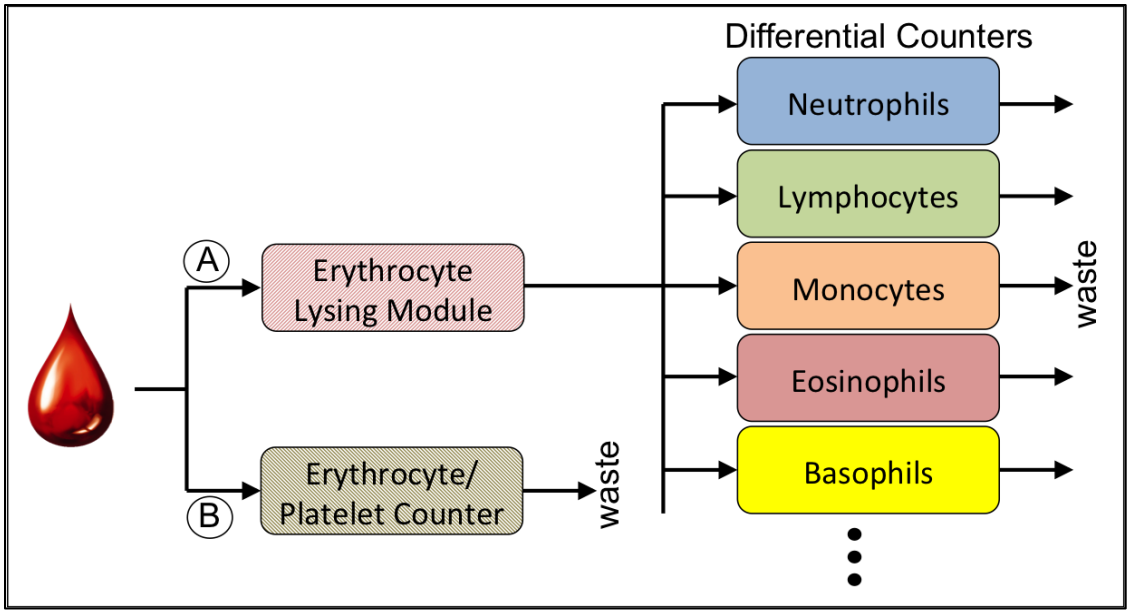

Figure 36: Block diagram of the complete cell count device based on the differential counting approach [36].

REFERENCES

[1] J. Wallach, *Interpretation of Diagnostic Test*s. 7th ed. Philadelphia, PA: Lippincott Williams & Wilkins, 2000.

[2] Invitrogen, "Flow cytometry tutorials: Introduction," April 2010. [Online]. Available: http://probes.invitrogen.com/resources/education/tutorials/4Intro Flow/player.html.

[3] S. Crowe, S. Turnbull, R. Oelrichs, and A. Dunne, "Monitoring of human immunode_ciency virus infection in resource-constrained countries," *Clinical Infectious Diseases*, vol. 37, pp. S25-S35, 2003.

[4] W. H. Coulter, "Means for counting particles suspended in a fluid," U.S. Patent no. 2,656,508, October 1953.

[5] IPTFM, "Particle Size Analysis by Electrical Sensing Zone Method (The Coulter Principle)," 2008. [Online]. Available: http://iptfm.com/zhuanli.asp?id=292.

[6] M. Koch, A. Evans, and A. Brunnschweiler, "Design and fabrication of a micromachined coulter counter," *Journal of Micromechanics and Microengineering*, vol. 9, pp. 159-161, 1999.

[7] Wikimedia, "Basis of Membrane Potential2.png," 2011. [Online]. Available: http://upload.wikimedia.org/wikipedia/commons/f/fb/Basis_of_Membrane_Potential2.png.

[8] P. Ellappan and R. Sundararajan, "A simulation study of the electrical model of a biological cell," *Journal of Electrostatics*, vol. 63, pp. 297–307, 2005.

[9] K.H. Schoenbach, S. Katsuki, R.H. Stark, E.S. Buescher, and S.J. Beebe, "Bioelectrics—New applications for pulsed power technology," *IEEE Transactions on Plasma Science,* vol. 30, no. 1, pp. 293-300, 2002.

[10] D. Holmes, D. Pettigrew, C.H. Reccius, J.D. Gwyer, C. Berkel, J. Holloway, D.E. Davies and H. Morgan, "Leukocyte analysis and differentiation using high speed microfluidic single cell impedance cytometry," *Lab on a chip,* vol. 9, pp. 2881–9, 2009.

[11] B.J. Kirby, *Micro- and Nanoscale Fluid Mechanics: Transport in Microfluidic Devices*. Cambridge University Press, 2010.

[12] A. Bard and L. Faulkner, *Electrochemical Methods*, 2nd ed. John Wiley & Sons, Inc., 2001.

[13] G.K. Batchelor, *An introduction to fluid dynamics*. Cambridge Mathematical Library (2nd ed.) Cambridge University Press, 2000.

[14] H.A Pohl, *Dielectrophoresis the behavior of neutral matter in nonuniform electric fields*. Cambridge University Press. Cambridge, 1978.

[15] M.P. Hughes, "AC electrokinetics: applications for Nanotechnology," *Nanotechnology,* vol. 11, pp.124–132, 2000.

[16] R. Tirumalai, K. Chan, D. Prieto, H. Issaq, T. Conrads, and T. Veenstra, "Characterization of the low molecular weight human serum proteome," *Molecular and Cellular Proteomics*, vol. 2, pp. 1096-1103, 2003.

[17] N.N. Watkins, S. Sridhar, X. Cheng, G.D. Chen, M. Toner, W. Rodriguez, R. Bashir, "A microfabricated electrical differential counter for the selective enumeration of CD4+ T lymphocytes," *Lab on a chip,* vol. 11, pp.1437–47, 2011.

[18] X. Cheng, Y. Liu, D. Irimia, U. Demirci, L. Yang, L. Zamir, W.R. Rodriguez, M. Toner, R. Bashir, "Cell detection and counting through cell lysate impedance spectroscopy in microfluidic devices," *Lab Chip,* vol. **7**, pp. 746–755, 2007.

[19] A. Pierzchalski, M. Hebeisen, A. Mittag, M.D. Berardino, A. Tarnok, "Label-free single cell analysis with a chip-based impedance flow cytometer," *Proc. of SPIE,* 7568, 75681B, 2010.

[20] G.S. Kampmann, A. Huwiler, M. Hebeisen, T. Hessler, M. Di Berardino, "On-chip non-invasive and label-free cell discrimination by impedance spectroscopy," *Cell Prolif,* vol. 41, pp. 830–840, 2008.

[21] K.C. Cheung, M. Di Berardino, G. Schade-Kampmann, M. Hebeisen, A. Pierzchalski, J. Bocsi, A. Mittag, A. Ta´rnok, "Microfluidic Impedance-Based Flow Cytometry," *Cytometry Part A,* vol. 77A, pp. 648-666, 2010.

[22] N.N. Watkins, U. Hassan, G. Damhorst, H. Ni, W. Rodriguez, R. Bashir, "An Integrated CD4+ and CD8+ T Lymphocyte Counter for Point-of-Care HIV/AIDS Diagnostics from Whole Blood," *Sci. Trans. Med.*, submitted, 2013.

[23] U. Hassan, P. Bajaj, G. Damhorst, R. Bashir, "Biomedical Micro and Nanotechnology: From Lab-on-Chip to Building Systems with Cells," *Conference Transducers 2013*, submitted, 2013.

[24] A.F.P. van Putten, S. Middelhoek, "Integrated silicon anemometer," *IEEE Electron. Lett*, vol. 10, pp. 425–426, 1974.

[25] H. Ernst, A. Jachimowicz and G. A. Urban, "High resolution flow characterization in Bio-MEMS," *Sens. Actuators A*, vol. 100, no. 1, pp. 54-62(9), 2002.

[26] T. Nakagama, T. Maeda, K. Uchiyama, and T. Hobo, "Monitoring nano-flow rate of water by atomic emission detection using helium radio-frequency plasma," *The Analyst*, vol. 128, pp. 543–546, 2003.

[27] R. Kliese, Y. Lim, E. Stefan, J. Perchoux, S. Wilson, and A. Rakić, "Rapid scanning flow sensor based on the self-mixing effect in a VCSEL," *2010 Conference on Optoelectronic and Microelectronic Materials and Devices (COMMAD),* pp. 7–8, Canberra, Australia, Dec. 2010.

[28] H.E. Ayliffe and R.D. Rabbitt, "An electric impedance based microelectromechanical system flow sensor for ionic solutions," *Meas Sci Technol.,* vol. 14, no.8, pp. 1321–1327, 2003.

[29] K. R. Visser, "Electrical conductivity of stationary and flowing human blood at low frequencies," *Med. & Biol. Eng. & Comput*., vol. 30, pp. 636-640, 1992.

[30] J. Collins and A. Lee, "Microfluidic flow transducer based on the measurement of electrical admittance," *Lab on a Chip,* vol. 4, pp. 7–10, 2004.

[31] E. D. Trautman, "A Practical Analysis of the Electrical Conductivity of Blood," *IEEE Trans. On Biomed. Engg.,* vol. no. 30, pp. 141-154, 1983.

[32] N.N. Watkins, U. Hassan, W. Rodriguez, and R. Bashir, "Electrical Flow Metering of Blood for Point-of-Care Diagnostics," *IEEE EMBC*, 2012, San Diego, CA.

[33] World Health Organization, *Global HIV/AIDS Response: Epidemic update and health sector progress towards Universal Access*, 2011.

[34] X. Cheng, A. Gupta, C. Chen, R.G. Tompkins, W. Rodriguez, and M. Toner, "Enhancing the performance of a point-of-care CD4+ T-cell counting microchip through monocyte depletion for HIV/AIDS diagnostics," *Lab on a chip,* vol. 9, pp. 1357–64, 2009.

[35] Y.N. Wang, Y. Kang, D. Xu, C.H. Chon, L. Barnett, S.A. Kalams, D. Li, "On-chip counting the number and the percentage of CD4+ T lymphocytes," *Lab on a chip*, vol. 8, pp. 309–15, 2008.

[36] CLIAwaived, "CBC (Hematology) Systems," 2003. [Online]. Available: http://www.cliawaived.com/web/CBC_(Hematology)_Systems.htm

APPENDIX DATA ANALYSIS

A.1. Pulse Counting Based on Threshold

```
function [timea amplitude] = cell_hist_dualfreq(file,th,f,flow)
% file is data
% th is the user selected threshold value
% f is the sampling frequency in kHz
% flow is the total flow rate
% timea is the width of the pulse
% amplitude is the maximum amplitude of the pulse for a particular threshold

fs = f/2;
b0 = file;
clear file

% High pass filter
[b, a] = butter(4,20/fs,'high');
b1 = filtfilt(b, a, b0);
clear b0 b a

% Band pass filter
[ba, aa] = butter(1,[59.5/fs 60.5/fs],'stop');
b2 = filtfilt(ba, aa, b1);
clear b1 ba aa

% Band stop filter
[baa, aaa] = butter(1,[119.5/fs 120.5/fs],'stop');
b3 = filtfilt(baa, aaa, b2);
clear b2 baa aaa
b = b3;
clear b3

%%%% base line correction
f = 1;
gap = 275;

for i=1:length(b)/gap
   z = b(f:i*gap);
   m = mean(z);
   z1 = z - m;
   data(f:i*gap) = z1;
   f = f+gap;
```

```
end
clear b
data = data';

%%%%% cell counting
k = 0;
x = 1;
counter = 0;
jj = 1;
time_diff = 0;
diff = 0;
fe = 0;
cc  =  0;

%for upward pulse analysis
if(th>0)
 for i = 1:length(data)-10
   %c = 0;
   if (i>k)
      if(data(i)>th)
         ini(x) = i;
         c = i;
         %for cc = 1:100
         cc = 0;
         while( (c+cc) ~= length(data)-10 )
            cc = cc + 1;
            if (data(c+cc)<th)
               if(cc>=3)
                  fin(x) = c+cc;
                  fe = fin(x);
                  break
               end
            end
         end

         amplitude(x) = max( data( ini(x):fin(x) ) );
         timea(x) = ini(x) + ( find(data( ini(x):fin(x) ) == amplitude(x)) ) - 1;
         time_diff(x) = 1 + (fin(x)-ini(x));
         if (time_diff(x)>30 )
            k =  fe+20;
            x = x;
         else
            k =  fe+1;
            x = x + 1;
         end
```

```
      end

   end

end
end

%for downward pulse analysis
if(th<0)
  for i = 1:length(data)-10
      if (i>k )
      if(data(i)<(th))
         ini(x) = i;
         c = i;

         cc = 0;
         while( (c+cc) ~= length(data)-10 )
            cc = cc + 1;
            if (data(c+cc)>th)
               fin(x) = c+cc;
               fe = fin(x);
               break;
            end
         end

          amplitude(x) = min( data( ini(x):fin(x) ) );
          timea(x) = ini(x) + ( find(data( ini(x):fin(x) ) == amplitude(x)) )-1;
         time_diff(x) = 1 + (fin(x)-ini(x));
         diff = time_diff(x);
         if (diff>30 )
            k =  fe+20;
            x = x;
         else
            k =  fe+1;
            x = x + 1;
         end

      end
   end
  end
end
end
```

A.2. Dual Frequency Measurement

```
function [time_fwd time_rev amp_fwd amp_rev] = dual_freq (data,indd,thres,fs,flow)


% for low freq measurements
% subtracting 100
   xx = find(data>=90,10);
   dat0 = data(xx(1):length(data))-100;
   dat00 = cat(2,data(1:xx-1),dat0);

   %time difference vs amplitude for forward counts
   dat1 = dat00(1:indd-100);
   [time_fwd amp_fwd] = cell_hist_dualfreq(dat1,thres,fs,flow);
   clear dat1
   %time difference vs amplitude for reverse counts
   dat2 = dat00(indd+200:length(dat00));
   clear dat00
   [time_rev amp_rev] = cell_hist_dualfreq(dat2,thres,fs,flow);
   clear dat2


end
```

A.3. Main Project File

```
clear all

auto = 0; %manually enter reverse file number and time within that file
%% Loading all TDMS files into memory
[data,index,name,LFfilepath,LFfilefolder] = readfile(auto); %NNW 2011-10-21

%% Take some inputs from USER
fsi = input('Please enter sampling frequency in kHz = ');
fs = fsi* 1000;

flow_input = input('Enter the flow rate (μL/min) = '); %NNW 2011-10-20

flow = flow_input/20; %normalize based on 20 μL/min flow rate

%%
dfile = input('If you are analyzing data files with a 100 shift, press y else press n:','s');
am = input('For auto reversal Press 1, For Manual press 2: ');

if (am==1)
```

```
    indd = reversal_detection(data);
else
    [indd] = reverse_index3(data,fs);
    end

ves  = 0;

for p = 1:length(index)
    index2(p) = index(p) + ves;
    ves = index2(p);
end

inddd = find(index2>indd);
fnum = inddd(1);
findex = indd - index2(inddd(1)-1);
rtime = findex/fs;



%% Dual Frequency Mesaurements
if (hi==3)
    thres = input('At what threshold you want to perform measurements:' );
    data_LF = data;
    clear data

    %input the new HF set of data files
    filepathfilter = strcat(LFfilefolder,'*MHz*.tdms'); %NNW 2012-02-23
    [filepath,filefolder]=uigetfile({filepathfilter},'Select TDMS Files (more than 1
necessary)','MultiSelect','on');   %NNW 2012-02-23


    [time_fwd_LF time_rev_LF amp_fwd_LF amp_rev_LF] = dual_freq
(data_LF,indd,thres,fs,flow);
    clear data_LF

    %input the new HF set of data files
    [data1,index,name1] = readfile_dual(auto,filepath,filefolder);

    xx = find(data1>=90,10);
    dat0 = data1(xx(1):length(data1))-100;
    dat00 = cat(2,data1(1:xx-1),dat0);
    clear dat0
    clear data1


    data_fwd_HF = filters_BL(dat00(1:indd-100),fs);
```

```
data_fwd_HF = data_fwd_HF';
data_rev_HF = filters_BL(dat00(indd+200:length(dat00) ),fs);
data_rev_HF = data_rev_HF';
clear dat00


   for p = 1:length(time_fwd_LF)
   amp_fwd_HF(p) = max (data_fwd_HF(time_fwd_LF(p)-5:time_fwd_LF(p)+5));
   %amp_rev_HF(p) = max (data_rev_HF(time_rev_LF(p)-15:time_rev_LF(p)+15));
end
clear data_fwd_HF
for p = 1:length(time_rev_LF)
   amp_rev_HF(p) = max (data_rev_HF(time_rev_LF(p)-5:time_rev_LF(p)+5));
end
clear data_rev_HF

Opacity_fwd = amp_fwd_HF ./ amp_fwd_LF;
Opacity_rev = amp_rev_HF ./ amp_rev_LF;

of = min(Opacity_fwd);
of1 = find(Opacity_rev>of);
Opacity_rev = Opacity_rev(of1);
amp_rev_LF = amp_rev_LF(of1);
amp_rev_HF = amp_rev_HF(of1);

HF_rev = amp_rev_HF;
LF_rev = amp_rev_LF;
HF_fwd = amp_fwd_HF;
LF_fwd = amp_fwd_LF;
clear amp_rev_HF
clear amp_rev_LF
clear amp_fwd_HF
clear amp_fwd_LF

 fwd_index = length(Opacity_fwd);
 rev_index = length(Opacity_rev);
 write_scatter_fwd(name, fwd_index, LF_fwd, HF_fwd, Opacity_fwd);
 %scatter3 for manual scaling
 HF_scale_fwd = 1024/0.6;
 HF_data_fwd =  HF_fwd .* HF_scale_fwd;
 clear HF_fwd

 LF_scale_fwd = 1024/2;
 LF_data_fwd =  LF_fwd .* LF_scale_fwd;
 clear LF_fwd
```

```
    Opacity_scale_fwd = 1024/(mean(Opacity_fwd)+(3*std(Opacity_fwd)));
    Opacity_data_fwd =  Opacity_fwd .* Opacity_scale_fwd;
    clear Opacity_fwd

    write_scatter_scaled_manual2(name,'fwd', fwd_index, LF_data_fwd, HF_data_fwd,
Opacity_data_fwd);
    clear LF_data_fwd HF_data_fwd Opacity_data_fwd

    write_scatter_rev(name, rev_index, LF_rev, HF_rev, Opacity_rev);
    HF_scale_rev = 1024/0.6;
    HF_data_rev =  HF_rev .* HF_scale_rev;
    clear HF_rev
    LF_scale_rev = 1024/2;
    LF_data_rev =  LF_rev .* LF_scale_rev;
    clear LF_rev

    Opacity_scale_rev = 1024/(mean(Opacity_rev)+(3*std(Opacity_rev)));
    Opacity_data_rev =  Opacity_rev .* Opacity_scale_rev;
    clear Opacity_rev

    write_scatter_scaled_manual2(name, 'rev',rev_index, LF_data_rev, HF_data_rev,
Opacity_data_rev);
end
```